Letter

Effect of symmetry breaking on short-wavelength acoustic phonons in the chiral magnet MnSi

Y. Nii,[1,2,*] Y. Hirokane,[3] T. Koretsune,[4] D. Ishikawa,[5] A. Q. R. Baron,[5] and Y. Onose[1]

[1]*Institute for Materials Research, Tohoku University, Sendai 980-8577, Japan*
[2]*PRESTO, Japan Science and Technology Agency (JST), Kawaguchi 332-0012, Japan*
[3]*Department of Basic Science, University of Tokyo, Tokyo 153-8902, Japan*
[4]*Department of Physics, Tohoku University, Aoba-ku, Sendai, Miyagi 980-8578, Japan*
[5]*Materials Dynamics Laboratory, RIKEN SPring-8 Center, 1-1-1 Kouto, Sayo, Hyogo 679-5148, Japan*

(Received 9 April 2021; revised 15 June 2021; accepted 16 July 2021; published 4 August 2021)

We have investigated the effects of spatial-inversion and time-reversal symmetry breaking on the acoustic phonon branches in chiral MnSi using high-resolution inelastic x-ray scattering and first-principles calculations. We find a momentum-transfer-dependent (***q***-dependent) splitting between transverse phonon bands having angular momentum parallel or antiparallel to ***q***. This is understood by a phenomenological theory using a gyrotropic tensor. We observed no significant impact from the time-reversal symmetry breaking induced by a magnetic field (energy shifts < 0.3 meV). This suggests the effect of time-reversal symmetry breaking is small or is restricted to a very-low-energy regime in this material, possibly due to small spin-orbit interaction.

DOI: 10.1103/PhysRevB.104.L081101

Symmetry breaking has been a fundamental concept in condensed-matter physics related to the emergence of novel electronic states [1]. In particular, spatial-inversion symmetry (SIS) and time-reversal symmetry (TRS) breaking lift the spin degeneracy of the electronic state. Therefore, novel spin-related phenomena emerge in symmetry-broken materials. The simplest case is a ferromagnet, in which broken TRS induces exchange splitting and gives rise to phenomena such as magnetoresistance, the anomalous Hall effect, and the optical Faraday effect [2]. The breaking of SIS also induces spin splitting through spin-orbit interaction, in which spin polarization depends on the momentum direction. For this reason, Rashba [3] or Dresselhaus [4] spin textures appear in the band structure of a wide range of noncentrosymmetric materials, giving rise to unique electromagnetic phenomena such as the Edelstein effect [5]. In this paper we investigate the effect of symmetry breaking on phononic bands.

It has been well known that the circularly polarized states of acoustic waves are realized in symmetry-broken materials such as chiral materials [6] and (anti-)ferromagnets [7,8]. These are understood as acoustic analogs of natural activity and the Faraday effect. The degeneracy of two transverse acoustic modes is lifted by the symmetry breaking, and as a result, circularly polarized eigenstates are realized. The mode splitting has been directly observed by inelastic neutron scattering (INS) in several chiral materials [9,10].

Recently several studies unveiled intriguing spin-related phononic phenomena in symmetry-broken materials such as phonon Hall effect [11–15], nonreciprocal thermal [16] and acoustic [17–19] transport, and magnetization control by phonons [20]. For understanding them, it is useful to regard the circularity of polarization as phonon angular momentum [21–23]. The concept of phonon angular momentum was first introduced by Vonsovskii and Svirskii in 1962 [21,22] and rediscovered by Zhang and Niu [24]. The phonon angular momentum may be taken as [23,24]

$$\boldsymbol{J}_{\mathrm{ph}} = \sum_{\alpha} \boldsymbol{u}_{\alpha} \times \boldsymbol{p}_{\alpha}, \tag{1}$$

where $\boldsymbol{u}_{\alpha}$ is displacement vector of the αth atom at about equilibrium position and $\boldsymbol{p}_{\alpha}$ is its momentum. $\boldsymbol{J}_{\mathrm{ph}}$ behaves as an internal degree of freedom of the phonon. By the introducing phonon angular momentum, the circularity of phonon polarization can be treated quantitatively, and intensive studies have been performed from the viewpoints of this concept [25–31]. In this context, revisiting phonon spectra in a symmetry-broken material is of fundamental importance to unveil how $\boldsymbol{J}_{\mathrm{ph}}$ is activated by symmetry breaking and to further develop these $\boldsymbol{J}_{\mathrm{ph}}$-related phenomena.

Here we study the effects of TRS and SIS breaking on the phononic band in a chiral magnet, MnSi, by means of a high-resolution inelastic x-ray scattering (IXS) [32] and first-principles calculations. We show the momentum-dependent splitting of phonon band is induced by SIS breaking. In contrast, the impact of TRS breaking on phonon energy was found to be negligibly small on the meV energy scale. These observations imply that the SIS breaking directly affects the phonon band but the effect of TRS breaking is only indirect, mediated by the small spin-orbit interaction, in contrast to the electronic cases.

MnSi belongs to the cubic chiral space group $P2_13$, and extensive studies have been performed for the past decade to investigate its topological skyrmion spin texture [33,34]. While the nontrivial topology of the phonon band was studied theoretically [35] and experimentally [36] in this class of compounds MSi (M = Fe, Co, Mn, Re, Ru), angular-momentum-dependent splitting has not been reported [37].

*y.nii@imr.tohoku.ac.jp

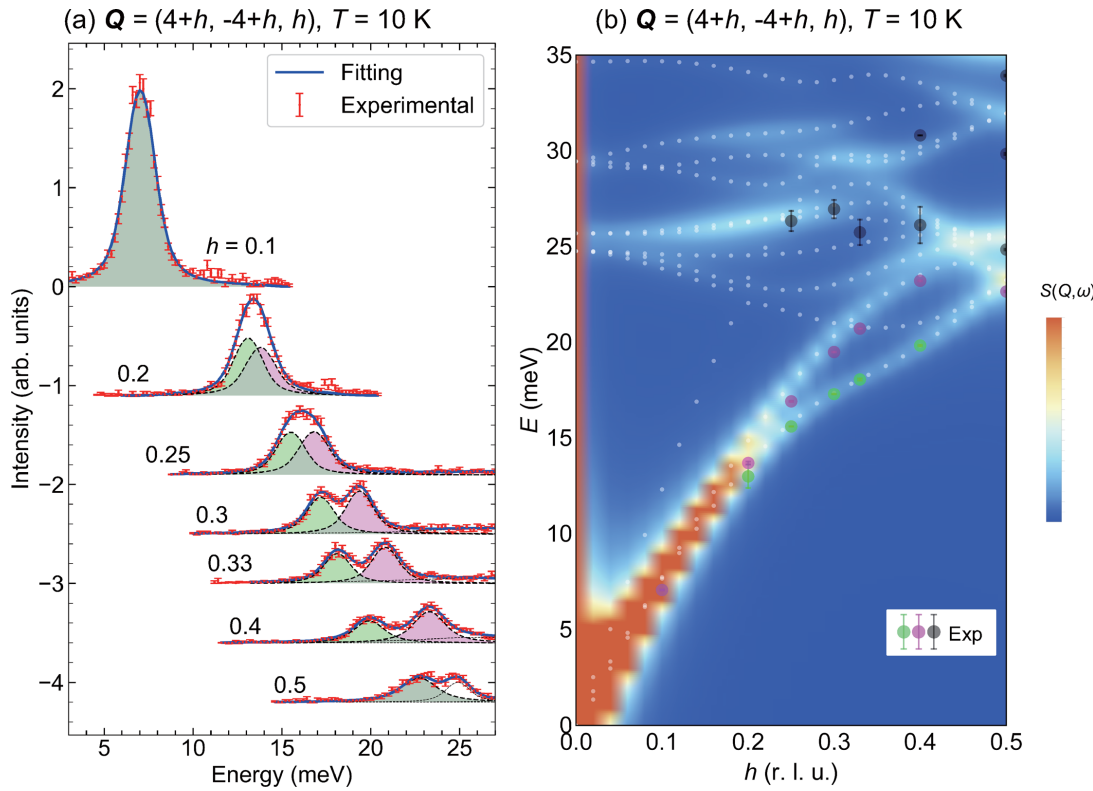

FIG. 1. (a) IXS profiles of MnSi along the high-symmetry line from a reciprocal lattice point (4, −4, 0) to R (4.5, −3.5, 0.5). These plots are offset for clarity. The IXS spectra are fitted to a sum of damped harmonic oscillator functions convoluted with an instrumental resolution function. (b) Comparison of experiment and calculation of IXS data. The color map and white dots represent the calculated dynamical structure factor $S(\boldsymbol{Q}, \omega)$ and phonon dispersions. The green, purple, and black circles represent experimental peak positions obtained from the fitting of IXS spectra as shown in (a).

In the present study, high-resolution IXS measurements were carried out at BL43LXU [32,38] of SPring-8 in Japan. The instrumental energy resolution was 1.4 meV FWHM. A single crystal of MnSi was grown by the floating-zone method in Ar gas. The sample was cut and carefully polished to be a thin plate shape of $2.4\times1.8\times0.14\,\mathrm{mm}^3$. Before the IXS measurement, the sample was annealed at 1173 K for 3 h in a vacuum to remove internal stress. The sample was mounted in a cryostat with a superconducting magnet and measured in a transmission geometry. For analysis of IXS data, a phonon band calculation was performed using density functional theory and the frozen phonon method with the VASP [39] and PHONOPY [40] packages. The plane-wave basis set with the projector augmented wave scheme [41] with a cut-off energy of 520 eV and Perdew-Burke-Ernzerhof (PBE) exchange-correlation functional [42] were used. For the frozen phonon calculation, a $3\times3\times3$ supercell was employed.

Figure 1(a) shows IXS spectra for various phonon wave vectors around (4, −4, 0). As the momentum is increased along the (111) reciprocal vector, a single broad peak tends to split, as shaded by green and purple colors, and the splitting energy becomes larger. To study the origin of these peaks, we show the calculated phonon dispersions and dynamical structure factor $S(\boldsymbol{Q}, \omega)$ in Fig. 1(b). Fitting and calculation procedures are shown in the Supplemental Material [43]. At the measured momentum transfers $(4+h, -4+h, h)$, the dynamical structure factor of the longitudinal mode is small and the observed peaks correspond to the transverse modes. If there are both SIS and TRS, two transverse acoustic modes propagating along the ⟨111⟩ direction should be degenerate (see Supplemental Material [43]). Because TRS breaking hardly affects the phononic spectra in this system as discussed later, the peak splitting seems to be caused by SIS breaking. This splitting was confirmed by our fits: even when the finite momentum resolution [Δh, Δk, $\Delta l \sim 0.02$ (r.l.u.)] is included, we clearly observe first an increase in linewidth and then full mode separation for $h \gtrsim 0.2$. The calculations shown in Fig. 1(b) also show (though it is hard to see at low $\boldsymbol{q}$) corresponding nondegenerate dispersions of the transverse acoustic mode. Nevertheless, it should be noted that in the calculated spectra, the two transverse modes cross each other at $h \approx 0.09$. This crossing in the small-q region is probably caused by the artifact owing to the finite size of the supercell ($3\times3\times3$) in our calculation. In the larger q region, the calculation is quite consistent with the experimental data.

To investigate the origin of the mode splitting, we plot $\boldsymbol{J}_{\mathrm{ph},\sigma}(\boldsymbol{q})$ in Fig. 2, which is the angular momentum of a phonon for the σth phonon branch and at wave vector $\boldsymbol{q}$ determined from our calculations. The ith component of $\boldsymbol{J}_{\mathrm{ph},\sigma}(\boldsymbol{q})$ can be obtained by $J^i_{\mathrm{ph},\sigma}(\boldsymbol{q}) = \hbar\epsilon^\dagger_\sigma(\boldsymbol{q})M_i\epsilon_\sigma(\boldsymbol{q})$, where $\boldsymbol{\epsilon}_\sigma(\boldsymbol{q})$ is the phonon polarization vector of the σth branch at wave vector $\boldsymbol{q}$, and the matrix M_i is given by $(M_i)_{jk} = I_{N\times N}\times(-i)\varepsilon_{ijk}$ for N atoms in a unit cell [24,31]. $I_{N\times N}$ represents the $N\times N$ identity matrix, and ε_{ijk} is the Levi-Civita symbol. $\boldsymbol{J}_{\mathrm{ph}}$ points

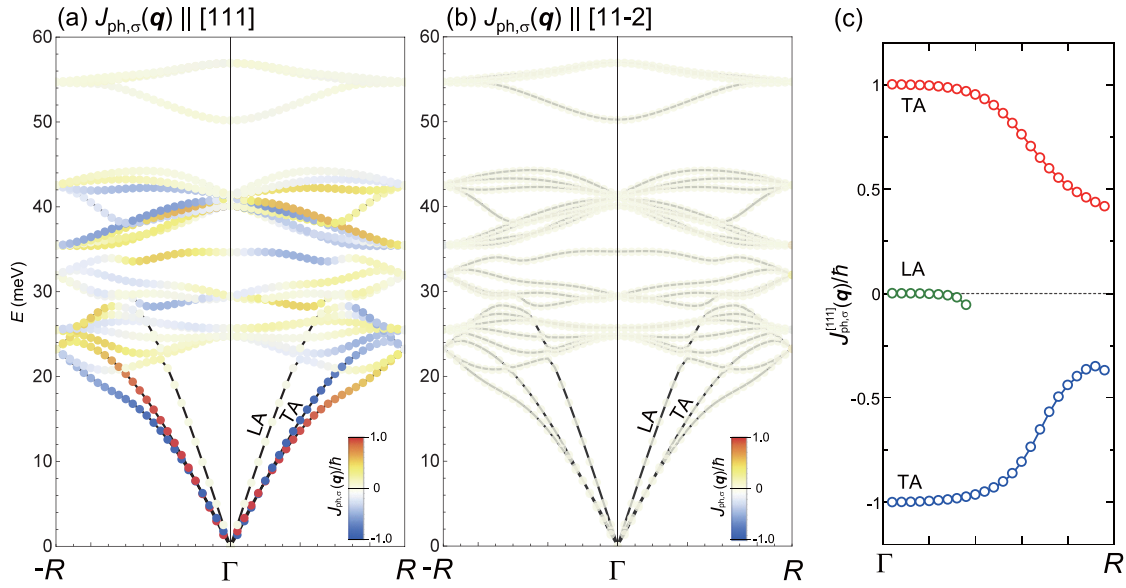

FIG. 2. Projections of the phonon angular momentum into (a) the [111], parallel and (b) [11-2], perpendicular direction for dispersion along the [111] direction (Γ-*R*). LA and TA indicate longitudinal and transverse acoustic modes, respectively. (c) Magnitude of phonon angular momentum along the [111] direction for the lowest three branches. In the small-q region, these three modes correspond to two TA modes and one LA mode, respectively. For the third lowest mode (LA mode), the data above $q = 0.2$ (r.l.u.) for (q, q, q) are omitted because of the mixing with optical modes.

parallel or antiparallel to the (h, h, h) wave vector for the transverse modes, while $\boldsymbol{J}_{\rm ph}$ of the longitudinal mode is negligible. Importantly, $\boldsymbol{J}_{\rm ph}$ is an odd function of the wave vector. Figure 2(c) quantitatively shows the magnitude of phonon angular momenta along the [111] direction from the Γ to *R* point. Here we plot only the lowest three branches, which correspond to two TA and one LA modes in the small-q region. This clearly presents that phonon angular momenta for the two TA modes are $\hbar$ and $-\hbar$, while that of the LA mode is negligible in the small-q region. The emergence of the $\boldsymbol{J}_{\rm ph}$ and TA mode splitting are closely related in the cubic lattice, as discussed in the Supplemental Material [43] (see also Ref. [44] therein). A similar spin splitting of the electronic state was observed in a chiral semiconductor Te [45]: the spin direction on the split Fermi surface is parallel or antiparallel to the momentum. In this sense the observed mode splitting is an indication of the phonon version of spin-momentum locking owing to the SIS breaking. It should be noted that this is also consistent with the well-known concept of acoustic natural activity [6], because the rotational direction of polarization is reversed upon a reversal of propagation direction in this phenomenon.

Let us consider splitting of the phonon mode in MnSi based on a phenomenological theory proposed by Portigal and Burstein [46]. According to their theory, elastic constants can be expanded in a power series of wave vector $\boldsymbol{q}$ as

$$C_{ij}(\omega, \boldsymbol{q}) = C_{ij}(\omega) + i d_{ijk} q_k + \cdots , \tag{2}$$

where the first term is the conventional elastic constant represented in Voigt notation, and the coefficient d_{ijk} is called the acoustic gyrotropic tensor [46]. The second term is present only in materials without SIS and is responsible for acoustic activity [6]. For transverse acoustic waves propagating along the [111] direction, one can obtain eigenfrequencies for these waves by solving Christoffel's equation [47]:

$$\omega_{\pm} = \sqrt{\frac{C \pm dq}{\rho}} q \simeq v_0 q \pm v_0 \left(\frac{d}{2C} \right) q^2. \tag{3}$$

Here $d = (3d_{152} - 3d_{163} - 2d_{453})/9$ and $C = (C_{11} - C_{12} + C_{44})/3$. $\rho = 5.833[\mathrm{g/cm^3}]$ is the density of MnSi, and $v_0 = (C/\rho)^{1/2}$ is the average velocity of transverse modes. The $\pm$ sign corresponds to the two counter-rotating, circularly polarized eigenmodes. Thus, Eq. (3) means that degeneracy of transverse modes is lifted by SIS breaking and eigenstates with circular polarization appear. To examine the validity of this phenomenological relation, we plot the energy splitting against the square of wave vector normalized by that of the Brillouin zone edge $q/q_{\rm BZ}$ in Fig. 3. The q^2 law is very well satisfied for the experimental results of MnSi, at least up to $q/q_{\rm BZ} = 0.66$ (i.e., $(q/q_{\rm BZ})^2 \approx 0.44$ and $q = 0.33$). From the slope of this plot and the elastic constant [48], the experimental acoustic gyrotropic tensor is estimated as $d = 9.86$ [Pa m]. Figure 3 also shows the result of the first-principles calculation. While a small dip was discerned in the small-q range owing to the aforementioned artifact caused by the finite cell size, the linear relation seems satisfied in the intermediate q range $[0.1 < (q/q_{\rm BZ})^2 < 0.4]$. The slope is larger than the experimental data ($d = 16.6$ [Pa m]). For comparison, experimental values [9,10] of other chiral materials are also shown. The size of energy splitting is the largest for MnSi, and compared with the other materials, the phenomenological theory is valid to higher momentum transfers. This seems partly due to the small unit cell and relative simplicity of MnSi: MnSi is useful for examining the validity of the phenomenological theory.

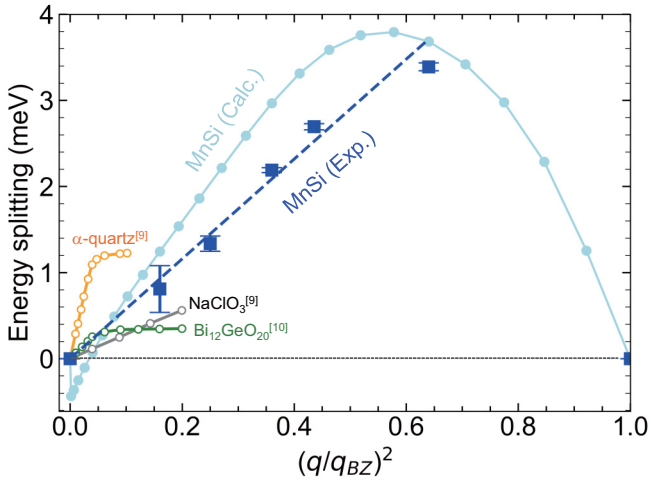

FIG. 3. Experimental and calculated energy difference of acoustic phonon modes for MnSi as a function of the square of the wave vector normalized by that at the Brillouin zone edge. The dip in the small-q region of the theoretical data is probably caused by the artifact owing to the calculation based on the finite size of the supercell (3×3×3). The experimental results of some other chiral materials [9,10] are also shown for comparison.

Finally, let us discuss the effect of TRS breaking. The TRS breaking is related to magnetism, but the coupling between the magnetism and phonons is nontrivial. Recently several novel phenomena induced by the phonon-magnetism coupling, such as the thermal phonon Hall effect [11–15], were observed. Therefore it is interesting to determine if phonon-magnetism coupling affects the phonon dispersion. In particular, some theories that explain the phonon Hall effect propose a so-called Raman-type phonon-magnetism interaction originating from spin-orbit interaction [49,50]:

$$H_{\mathrm{Raman}} = K\boldsymbol{s}\cdot\boldsymbol{J}_{\mathrm{ph}}, \tag{4}$$

where $\boldsymbol{s}$ is a spin moment and K is the coupling coefficient. If this interaction is valid in MnSi, one should observe an energy shift depending on both momentum and magnetization. To examine this we measured the magnetic field dependence of the acoustic phonon modes. Figure 4(a) displays IXS spectra showing transverse phonon modes at $\mathbf{Q} = (4.33, -3.67, 0.33)$ at 10 K with and without magnetic field. This comparison shows no discernable change even at ±0.7 T, where the magnetization is almost saturated as shown in Fig. 4(b). In Fig. 4(c) the peak energies are plotted against the magnetic field. They show almost no magnetic field dependence: energy shifts are less than 0.3 meV, the energy differences between the two modes changes by <0.15 meV, and there is no tendency to follow the magnetization curves, as shown in Fig. 4(d).

In previous works, enhanced phonon-magnetism coupling was observed in the magnetic resonance frequency range (GHz frequency ∼10 μeV) in some transition-metal compounds [7,8,18,26] or devices [17,19], leading to energy shifts of ∼1 μeV. The magnetic resonance of MnSi was observed at GHz range [51], and magnon energy at the finite wave vector is also limited to lower energy than that of the phonon [52]. Therefore a relatively large effect of phonon-magnetism coupling through hybridization with these magnetic excitations

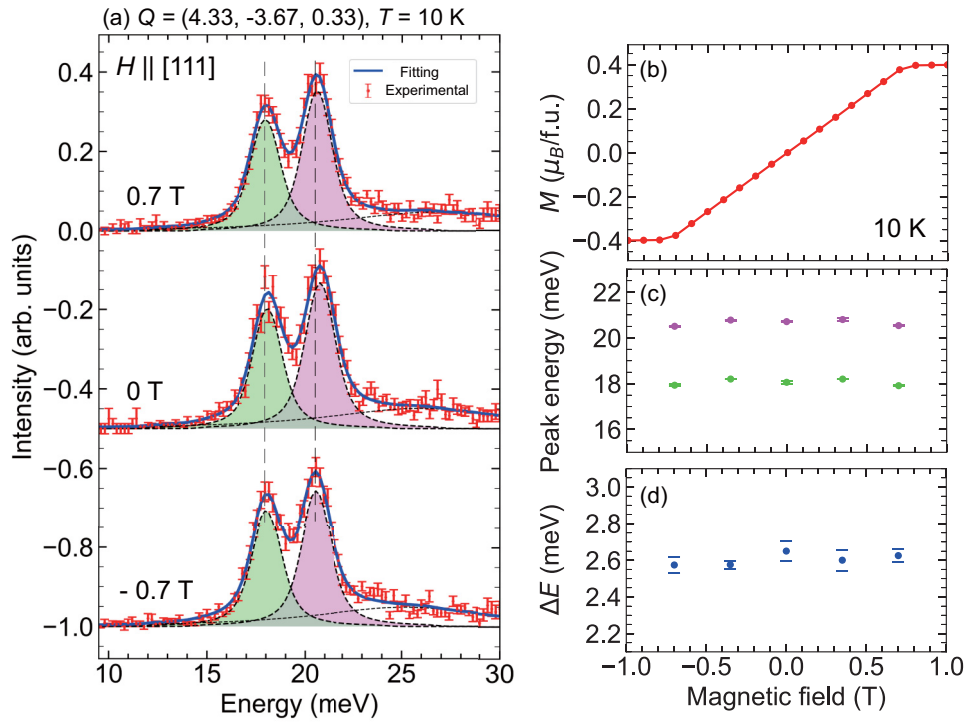

FIG. 4. Magnetic field dependence of transverse acoustic modes. (a) IXS spectra at 0 T and ± 0.7 T, 10 K, and $\mathbf{Q} = (4+h, -4+h, h)$ at $h = 0.33$. A magnetic field is applied along [111], which is parallel to $\boldsymbol{J}_{\mathrm{ph}}$. (b) Magnetization curve at 10 K along the [111] direction. (c), (d) Magnetic field dependence of (c) these peak energies and (d) difference between the energies.

may be restricted to the low-energy regime in transition-metal compounds. On the other hand, in the case of a rare-earth compound CeF_3, a large ($\sim$3 meV) magnetic field effect has been observed for high-energy optical phonon modes due to the relatively large spin-orbit interaction of rare-earth ions [53]. Incidentally, nonreciprocal thermal transport has been observed below the ordering temperature of the Tb $4f$ moment for a multiferroic $TbMnO_3$, which requires the effect of TRS breaking on a wide energy scale [16]. While the effect of TRS breaking on the phononic system seems appreciable even apart from the magnetic resonance frequency in the case of $4f$ electron systems with strong spin-orbit interaction, it is within the experimental resolution in the present transition-metal case.

To summarize, we have investigated the effects of SIS and TRS breakings on the phononic dispersion in MnSi. We reveal that the twofold degeneracy of transverse acoustic modes are lifted owing to the chirality at a finite wave vector. In agreement with the phenomenological theory, the energy splitting was found to be proportional to q^2. On the other hand, broken TRS has little impact on chiral phononic states, which indicates that the effect of phonon-magnetism coupling is small or is restricted to a very-low-frequency range in this compound. In electronic systems, the effect of TRS breaking is much more noticeable, for example, as ferromagnetic exchange splitting in a spectrum, while the impact of SIS breaking is mediated by the small spin-orbit coupling. In contrast, in phononic systems the effect of SIS breaking is direct while that of TRS is induced by the small spin-orbit interaction. To observe the large impact of magnetism in phononic dispersion, larger spin-orbit coupling seems to be needed. Some rare-earth compounds show novel thermal phenomena induced by large phonon-magnetism coupling [15,16]. In these cases, the spin-orbit coupling is comparable or larger than the crystal field splitting. Perhaps the comparison of the spin-orbit interaction and crystal field effect is crucial for the phonon-magnetism coupled phenomena.

We thank Y. Tomioka for the help with crystal growth. This work is supported by JSPS KAKENHI (Grants No. JP18K13494 and No. JP20K03828), PRESTO (Grant No. JPMJPR19L6), and the Mitsubishi Foundation. The phonon measurements were performed at BL43LXU of the RIKEN SPring-8 Center.

[1] R. R. Briss, *Symmetry and Magnetism* (North-Holland, Amsterdam, 1966).
[2] S. Chikazumi, *Physics of Ferromagnetism*, 2nd ed. (Oxford University Press, Oxford, UK, 1997).
[3] E. I. Rashba, Sov. Phys. Solid State **2**, 1109 (1960).
[4] G. Dresselhaus, Phys. Rev. **100**, 580 (1955).
[5] V. M. Edelstein, Solid State Commun. **73**, 233 (1990).
[6] A. S. Pine, Phys. Rev. B **2**, 2049 (1970).
[7] H. Matthews and R. C. LeCraw, Phys. Rev. Lett. **8**, 397 (1962).
[8] M. Boiteux, P. Doussineau, B. Ferry, J. Joffrin, and A. Levelut, Phys. Rev. B **4**, 3077 (1971).
[9] C. Joffrin, B. Dorner, and J. Joffrin, J. Phys. Lett. **41**, 391 (1980).
[10] C. Lin, T. Fang, Z. Tai-yong, N. Shi-wen, G. Cheng, and S. Zhong-jian, Solid State Commun. **54**, 803 (1985).
[11] C. Strohm, G. L. J. A. Rikken, and P. Wyder, Phys. Rev. Lett. **95**, 155901 (2005).
[12] A. V. Inyushkin and A. N. Taldenkov, JETP Lett. **86**, 379 (2007).
[13] K. Sugii, M. Shimozawa, D. Watanabe, Y. Suzuki, M. Halim, M. Kimata, Y. Matsumoto, S. Nakatsuji, and M. Yamashita, Phys. Rev. Lett. **118**, 145902 (2017).
[14] T. Ideue, T. Kurumaji, S. Ishiwata, and Y. Tokura, Nat. Mater. **16**, 797 (2017).
[15] Y. Hirokane, Y. Nii, Y. Tomioka, and Y. Onose, Phys. Rev. B **99**, 134419 (2019).
[16] Y. Hirokane, Y. Nii, H. Masuda, and Y. Onose, Sci. Adv. **6**, eabd3703 (2020).
[17] R. Sasaki, Y. Nii, Y. Iguchi, and Y. Onose, Phys. Rev. B **95**, 020407(R) (2017).
[18] T. Nomura, X.-X. Zhang, S. Zherlitsyn, J. Wosnitza, Y. Tokura, N. Nagaosa, and S. Seki, Phys. Rev. Lett. **122**, 145901 (2019).
[19] M. Xu, K. Yamamoto, J. Puebla, K. Baumgaertl, B. Rana, K. Miura, H. Takahashi, D. Grundler, S. Maekawa, and Y. Otani, Sci. Adv. **6**, eabb1724 (2020).
[20] R. Sasaki, Y. Nii, and Y. Onose, Nat. Commun. **12**, 2599 (2021).
[21] S. V. Vonsovkii and M. S. Svirskii, Sov. Phys. Solid State **3**, 1568 (1962).
[22] A. T. Levine, Nuovo Cimento **26**, 190 (1962).
[23] A. G. McLellan, J. Phys. C: Solid State Phys. **21**, 1177 (1988).
[24] L. Zhang and Q. Niu, Phys. Rev. Lett. **112**, 085503 (2014).
[25] H. Zhu, J. Yi, M.-Y. Li, J. Xiao, L. Zhang, C.-W. Yang, R. A. Kaindl, L.-J. Li, Y. Wang, and X. Zhang, Science **359**, 579 (2018).
[26] J. Holanda, D. S. Maior, A. Azevedo, and S. M. Rezende, Nat. Phys. **14**, 500 (2018).
[27] X. Chen, X. Lu, S. Dubey, Q. Yao, S. Liu, X. Wang, Q. Xiong, L. Zhang, and A. Srivastava, Nat. Phys. **15**, 221 (2019).
[28] G. Grissonnanche, S. Theriault, A. Gourgout, M.-E. Boulanger, E. Lefrancois, A. Ataei, F. Laliberte, M. Dion, J.-S. Zhou, S. Pyon, T. Takayama, H. Takagi, N. Doiron-Leyraud, and L. Taillefer, Nat. Phys. **16**, 1108 (2020).
[29] K. Y. Bliokh and V. D. Freilikher, Phys. Rev. B **74**, 174302 (2006).
[30] S. Park and B.-J. Yang, Nano Lett. **20**, 7694 (2020).
[31] M. Hamada, E. Minamitani, M. Hirayama, and S. Murakami, Phys. Rev. Lett. **121**, 175301 (2018).
[32] A. Q. R. Baron, in *Synchrotron Light Sources and Free-Electron Lasers: Accelerator Physics, Instrumentation and Science Applications*, edited by E. Jaeschke, S. Khan, J. R. Schneider, and J. B. Hastings (Springer International Publishing, 2016), pp. 1643–1757; see also A. Q. R. Baron, arXiv:1504.01098.
[33] S. Mühlbauer, B. Binz, F. Jonietz, C. Pfleiderer, A. Rosch, A. Neubauer, R. Georgii, and P. Böni, Science **323**, 915 (2009).
[34] X. Z. Yu, Y. Onose, N. Kanazawa, J. H. Park, J. H. Han, Y. Matsui, N. Nagaosa, and Y. Tokura, Nature (London) **465**, 901 (2010).
[35] T. Zhang, Z. Song, A. Alexandradinata, H. Weng, C. Fang, L. Lu, and Z. Fang, Phys. Rev. Lett. **120**, 016401 (2018).

[36] H. Miao, T. T. Zhang, L. Wang, D. Meyers, A. H. Said, Y. L. Wang, Y. G. Shi, H. M. Weng, Z. Fang, and M. P. M. Dean, Phys. Rev. Lett. **121**, 035302 (2018).
[37] D. Lamago, E. S. Clementyev, A. S. Ivanov, R. Heid, J.-M. Mignot, A. E. Petrova, and P. A. Alekseev, Phys. Rev. B **82**, 144307 (2010).
[38] A. Q. R. Baron, SPring-8 Inf, Newsl. **15**, 14 (2010), http://user.spring8.or.jp/sp8info/?p=3138.
[39] G. Kresse and D. Joubert, Phys. Rev. B **59**, 1758 (1999).
[40] A. Togo and I. Tanaka, Scr. Mater. **108**, 1 (2015).
[41] P. E. Blöchl, Phys. Rev. B **50**, 17953 (1994).
[42] J. P. Perdew, K. Burke, and M. Ernzerhof, Phys. Rev. Lett. **77**, 3865 (1996).
[43] See Supplemental Material at http://link.aps.org/supplemental/10.1103/PhysRevB.104.L081101 for fitting procedure of IXS spectra, calculation procedure of the dynamical structure factor, and symmetry considerations for transverse acoustic phonon modes.
[44] M. T. Dove, *Introduction to Lattice Dynamics* (Cambridge University Press, Cambridge, 1993).
[45] M. Sakano, M. Hirayama, T. Takahashi, S. Akebi, M. Nakayama, K. Kuroda, K. Taguchi, T. Yoshikawa, K. Miyamoto, T. Okuda, K. Ono, H. Kumigashira, T. Ideue, Y. Iwasa, N. Mitsuishi, K. Ishizaka, S. Shin, T. Miyake, S. Murakami, T. Sasagawa, and T. Kondo, Phys. Rev. Lett. **124**, 136404 (2020).
[46] D. L. Portigal and E. Burstein, Phys. Rev. **170**, 673 (1968).
[47] *Physical Acoustics, Principles and Methods*, edited by W. P. Mason (Academic Press, New York, 1964).
[48] Shear modulus C was derived from the averaged slope of phonon dispersion as $C = 114.1$ GPa from experiment and $C = 135.6$ GPa from calculation, respectively.
[49] T. Ray and D. K. Ray, Phys. Rev. **164**, 420 (1967).
[50] H. Capellmann and S. Lipinski, Z. Phys. B **83**, 199 (1991).
[51] M. Date, K. Okuda, and K. Kadowaki, J. Phys. Soc. Jpn. **42**, 1555 (1977).
[52] P. Böni, B. Roessli, and K. Hradil, J. Phys.: Condens. Matter **23**, 254209 (2011).
[53] G. Schaack, Solid State Commun., **17**, 505 (1975).